THE JOURNAL OF PHYSICAL CHEMISTRY C
A JOURNAL OF THE AMERICAN CHEMICAL SOCIETY

pubs.acs.org/JPCC

Article

Experimental and *Ab Initio* Study of Cu_2SnS_3 (CTS) Polymorphs for Thermoelectric Applications

Ketan Lohani, Himanshu Nautiyal, Narges Ataollahi, Carlo Fanciulli, Ilya Sergueev, Martin Etter, and Paolo Scardi*

Cite This: *J. Phys. Chem. C* 2021, 125, 178–188

Read Online

ACCESS | Metrics & More | Article Recommendations | Supporting Information

ABSTRACT: Cu_2SnS_3 (CTS) is a medium-temperature, ecofriendly, p-type thermoelectric material known for phonon-glass-electron-crystal characteristic. In the present work, ordered and disordered CTS samples were prepared from elemental powders, and their electronic and vibrational properties were systematically investigated by experimental methods and *ab initio* calculations. The disordered CTS polymorph presents a higher power factor, PF ~ 1.5 μW/K^2 cm, than the ordered and stable phase, PF ~ 0.5 μW/K^2 cm, above 700 K, as an effect of a smaller band gap and higher carrier concentration. Most importantly, the disordered CTS shows an ultralow thermal conductivity, k ~ 0.4−0.2 W/m K, as compared to ordered, k ~ 1.0−0.4W/m K, in the temperature range of 323−723 K. The combined effect of a higher PF and lower k results in a higher figure of merit, zT ~ 0.5 at 723 K, obtained for disordered CTS without resorting to chemical alloying. It turns out that structural disorder contributes to the suppression of thermal conductivity. While group velocity of acoustic phonons, as shown both by experiments and *ab initio* calculations, is similar in the two polymorphs, a strong anharmonicity characterizes the disordered CTS, resulting in the presence of low-lying optical modes acting as traps for heat transmission. Density functional theory/density functional perturbation theory simulations and nuclear inelastic scattering combined with high-resolution diffraction studies of the lattice parameters reveal details of phonon−phonon interactions in CTS with unprecedented effectiveness.

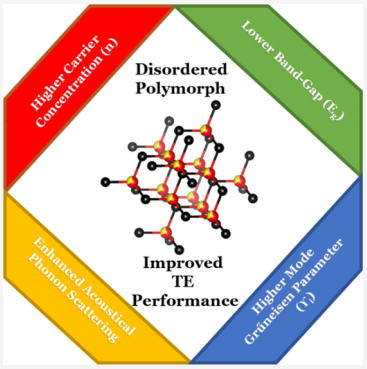

INTRODUCTION

Thermoelectric (TE) materials attract increasing interest in applications involving thermal gradients for durable, noise-free, and scalable solid-state power generators and coolers.[1−4] Performing TE devices require an optimal combination of properties—Seebeck coefficient (S), electrical conductivity (σ), and thermal conductivity (k)—to maximize the figure of merit, $zT = TS^2\sigma/k$. Therefore, an ideal TE material would require a high power factor (PF = $S^2\sigma$) and a low k (involving an electronic (k_e) and a lattice (k_l) component). In particular, obtaining an ultralow thermal conductivity is one of the main goals of the current research on TE materials.[5−7]

The Cu_2SnS_3 mineral phase was first reported in 1983, as a new sulfide with a triclinic structure (SG: $P1$).[8] It has been widely studied as an absorber material for photovoltaic devices owing to its high (~10^4 cm^{-1}) optical absorption coefficient and tunable band gap spanning from 0.7 to 1.6 eV.[9−13] In recent years, CTS has attracted interest from the TE community for its 3D hole conductive network and ultralow thermal conductivity, a so-called "phonon-glass-electron-crystal" characteristic.[14] At first, in 2016, Tan *et al.*[15] and Shen *et al.*[16] reported CTS as a potential TE material, using In and Zn doping, respectively. Other researchers have reported Mn,[17] Ni,[18] Fe,[19] and Co[20] doping to enhance the TE performance of CTS.

The experimental literature suggests that undoped CTS forms an ordered monoclinic (SG: Cc) phase.[21] However, this ordered CTS polymorph has high electrical resistivity (ρ) and k values, resulting in a low zT.[19] One way to lower k is to hinder the propagation of phonon waves [1], and to do this, some researchers produced a disordered cubic (SG: $F\bar{4}3m$) polymorph.[20] This, however, required acceptor cation doping, except in our recent work,[22] where we have shown how to stabilize the disordered CTS polymorph using a bottom-up (reactive milling) production technique that does not require any doping.

CTS polymorphs are a variant of the zinc blende (ZnS) structure (Figure 1a), made of tetrahedral cages (Figure 1b) of S (Wyckoff position 4c) with a cation (Zn) positioned in the middle (4a). For ordered (Figure 1c) and disordered (Figure 1d) CTS, the Zn cation is stoichiometrically replaced by Cu and Sn, respectively, in an ordered and in a random manner. This results in a partial cation occupancy of 2/3, and 1/3, for

Received: October 8, 2020
Revised: December 11, 2020
Published: December 30, 2020

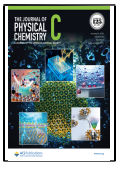

https://dx.doi.org/10.1021/acs.jpcc.0c09139
J. Phys. Chem. C 2021, 125, 178−188

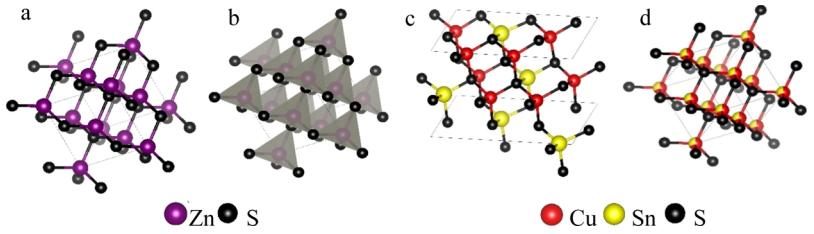

Figure 1. ZnS structure (a) with tetrahedral drawn (d) and monoclinic (SG: *Cc*) ordered (a), cubic (SG: $F\bar{4}3m$) disordered (b) CTS.

Cu and Sn, respectively.[23] These polymorphs can also be understood as an assembly of S coordination motifs, in which each S anion is connected to four (Cu/Sn) cations, making tetrahedral motifs. Zawadzki *et al.*[24] have put forward that cations in CTS structures contain five possible S−Cu_iSn_{4-i} motifs, where $i \in \{0, ..., 4\}$, but the S−Cu_4, S−$CuSn_3$, and S−Sn_4 motifs are energetically unlikely to form. The ordered CTS has a regular distribution of S−Cu_2Sn_2 and S−Cu_3Sn motifs, while in disorder CTS, S−Cu_2Sn_2 motifs form nanometer-scale clusters. Additionally, because the octet rule is not locally respected in these structures, all of this brings the crystal structure, especially in the disordered phase, close to instability. In the present work, the abovementioned clustering effect was not taken into account for *ab initio* calculations because of the limitation of computational resources, rather two, Sn-rich and Sn-poor disordered cells. Zhai *et al.*[25] have discussed the difficulty in the *ab initio* simulation of similar Cu_2SnX_3 (X = S/Se) disordered structures, and how this limits the electronic information from band structures. However, the electronic bands for the ordered phase are diffusely discussed in the literature.[25−27] In the similar CTSe system,[28] the disordered polymorph shows a lower band gap energy than the corresponding ordered phase, which promotes a higher carrier concentration (n), resulting in a higher PF. Recently, we have shown that the disordered CTS polymorph without acceptor doping presents a higher PF ∼ 1.1 $\mu W/K^2$ cm than the ordered polymorph, PF ∼ 0.1 $\mu W/K^2$ cm, above 700 K. In fact, the disordered polymorph has a lower Seebeck (S ∼ 250−325 $\mu V/K$) and resistivity (ρ ∼ 1.5−1.0 Ω cm) than the ordered polymorph (S ∼ 600−700 $\mu V/K$, ρ ∼ 27−30 Ω cm), in the temperature range of 323−723 K.[22]

Both polymorphs show a decreasing k trend with increasing temperature, indicating the presence of a dominating phonon−phonon interaction.[20] However, it is the ultralow thermal conductivity (k < 0.5 W/K m) shown by the disordered polymorph which is particularly interesting[17] and still little studied. Several mechanisms could be at the origin of this much-desired behavior, such as an enhanced phonon scattering because of the increase in crystal symmetry, cation disorder, soft bonds, alloy scattering, and possible suppression of normal phonon scattering process because of random cations and dopant distribution.[16,19]

In this work, ordered and disordered CTS polymorphs were produced in a highly controlled environment from elemental powders (Cu, Sn, and S) using a high-energy reactive ball-mill, followed by sintering at various temperatures. We started from the experimental results for PF and thermal conductivity for both the phases, stating the higher performance of the disordered form of CTS. Therefore, we have investigated the mechanisms leading to the improvements observed, looking for a full understanding of the CTS system. The work presents a unique mix of experimental analyses and theoretical calculations that are able to achieve a complete description of the CTS property dependence by the structural phase disorder. We have studied electronic and vibrational properties using density functional theory (DFT) and density functional perturbation theory (DFPT) simulations, respectively. The *ab initio* calculations provide insights on the possible origin of the ultralow k, which is identified as a distinct behavior of the cations in the disordered structure. By investigating the vibrational density of states (DOS) and phonon dispersion curves and correlating them with the mode Grüneisen parameters (γ_i) and electron localization function (ELF) curves, we unveil the vibrational properties of CTS. Nuclear inelastic scattering (NIS) from Sn provides direct experimental evidence on the vibrational DOS, validating the DFPT results, and in particular, the mechanism underlying the ultralow thermal conductivity of the cubic disordered CTS phase. Moreover, by combining NIS and high-resolution X-ray diffraction (XRD) measurements, Grüneisen parameters were experimentally calculated for the disordered sample. The investigation proposed in this work, covering most of the material characteristics, can be the base for the design of novel solutions for the development of materials based on CTS with improved TE properties.

MATERIAL AND METHODS

Experimental Methods. Elemental powders of Cu, Sn, and S, procured from Sigma-Aldrich (99% pure) were fed in ball-mill vials made of WC, and anhydrous C_2H_5OH (100 μlt.) was added to the mixture as a lubricant. High-energy ball-milling Fritsch P4 was used for the milling. The mill was operated for 30 and 60 min, with a fixed main disk and spinning speed of 300 rpm and −540 rpm, respectively. Two circular pellets (thickness ∼1.5 mm, diameter ∼16 mm) were prepared using a manual cold press. One sample was sintered at 500 °C, and the other was sintered at 650 °C, for 2 h in Ar flux. The entire synthesis process was performed in a highly controlled environment (O_2 and H_2O < 10 ppm).

XRD was performed on as-milled powders and sintered disks, in Bragg−Brentano geometry using a Rigaku PMG powder diffractometer equipped with a graphite bent-crystal monochromator, and Cu Kα source operated at 40 kV and 30 mA. The optical properties of CTS polymorphs were investigated using a PerkinElmer spectrophotometer (PerkinElmer, Milan, Italy), model LAMBDA 750, equipped with a 150 mm integrating sphere. The polycrystalline samples were dispersed in ethanol and sonicated for 1 h, and the optical absorption spectra were collected. Mobility (μ) and carrier concentration (n) were measured with an MMR K-20 and an H-50 measurement system by applying a magnetic field of 6720 Gauss, in temperature range 300−450 K. The absolute Seebeck coefficient (S) was measured using a Pt Standard, while resistivity (ρ) was measured by four-contact measure-

https://dx.doi.org/10.1021/acs.jpcc.0c09139
J. Phys. Chem. C 2021, 125, 178−188

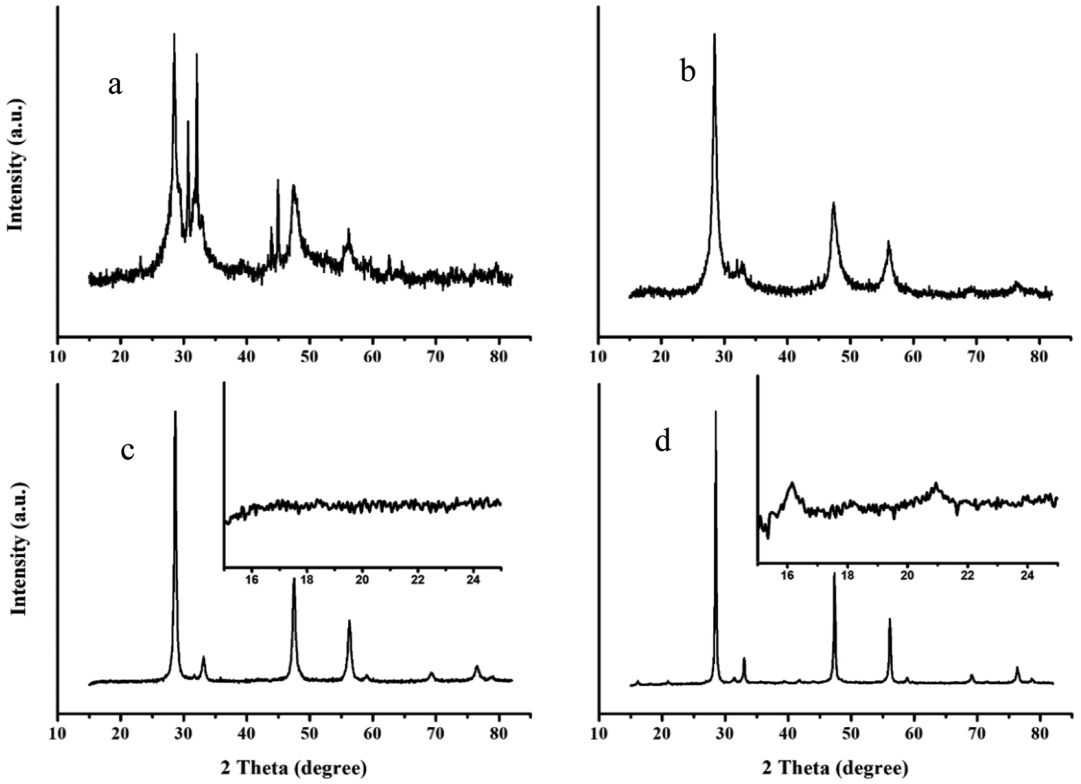

Figure 2. XRD pattern of CTS samples after 30 (a), and 60 min milling (b); then, in the sintered disordered (c) and ordered (d) forms. The insets show details of the distinctive peaks of the monoclinic phase.

ments using a Linseis LSR-3 instrument. Thermal diffusivity (D) was measured using a Linseis LFA-500. S, ρ, and D measurements were performed over the temperature range of 323−723 K. To verify our theoretical findings, we have used NIS with ^{119}Sn nuclear resonance. The method provides the partial phonon-DOS (pDOS) of Sn atoms. Experiments were carried out at the dynamics beamline P01 at PETRAIII (DESY, Hamburg) using a high-resolution monochromator with 1.4 meV energy resolution at 23.9 keV, the energy of the ^{119}Sn nuclear transition. The measurements were performed on samples with natural enrichment by ^{119}Sn (8.6%) inserted into the closed cycle He cryostat and kept at 43 and 295 K. The nuclear resonance signal was separated in time from electronic X-ray fluorescence and measured using a Si avalanche photodiode detector. This measurement was combined with high-resolution XRD studies of the lattice parameters between 100 and 300 K at the beamline P02.1 at PETRAIII. The combination of the phonon and lattice parameter measurements provides the possibility to obtain the mode Grüneisen parameters.

Computational Methods. The electronic structures were studied using DFT as implemented in the Vienna *ab initio* simulation package.[29,30] The interaction between the electron ion was described using the projector augmented wave method. The generalized gradient approximation with Perdew−Burke−Ernzerhof (PBE)[31] electron exchange−correlation was employed for band structure and DOS calculations.

The ternary ordered and disordered CTS polymorphs present Cc and $F\bar{4}3m$ structural symmetry, respectively. As already pointed out, in the ordered CTS, each S anion is tetrahedrally bonded by four cations (Cu/Sn), forming S−Cu_2Sn_2 and S−Cu_3Sn motifs. The disordered CTS system is possible when the cations (Cu/Sn) randomly replace Zn with an occupancy of 66.66 and 33.33%, respectively, in a diamond-like ZnS structure. This partial occupancy leads to a primitive cell that cannot be simulated exactly.[25] To satisfy the partial occupancy and respect the stoichiometry, one needs to make large cells that are computationally nonviable to solve. To overcome this limitation, two disordered cells were modeled by a slight alteration of the partial occupancy of Cu and Sn, respectively. The first cell was modeled with Cu (65.625%) and Sn (34.375%), and the second cell was modeled with Cu (68.75%) and Sn (31.25%). Hereafter, the first and second disordered cells are referred to as disordered Sn-rich and disordered Sn-poor, respectively.

The plane wave cutoff and electronic convergence were set to 500 eV and 10^{-6} eV, respectively. All the structures were relaxed until the force on each atom was <0.01 eV Å^{-1}, using a Gaussian smearing with σ = 0.05. Two k-point mesh of 4 × 3 × 4 and 4 × 4 × 4 were used for ordered and disordered systems, respectively, using the Monkhrost−Pack technique centered at the Γ-point.[32] For single-point self-consistent field calculation, the tetrahedron method and Blöchl corrections were considered. The high symmetry path was provided by SeekPath.[33] The DOS was calculated on a dense k-mesh of 12 × 12 × 12 and 8 × 8 × 8 grids.

The phonon dispersion curve and pDOS were calculated using the Phonopy[34] code. For DFPT calculations, local density approximation[35] was used with a 10^{-8} eV convergence criteria. These calculations were performed on the ordered supercell (2 × 2 × 2), whereas, for both the disordered cells, a much larger, 64-atom cell was used. The mode Grüneisen parameter (γ_i) was calculated using a quasi-harmonic approximation, by expanding and contracting the relaxed cell volume by ±1%.

https://dx.doi.org/10.1021/acs.jpcc.0c09139
J. Phys. Chem. C 2021, 125, 178−188

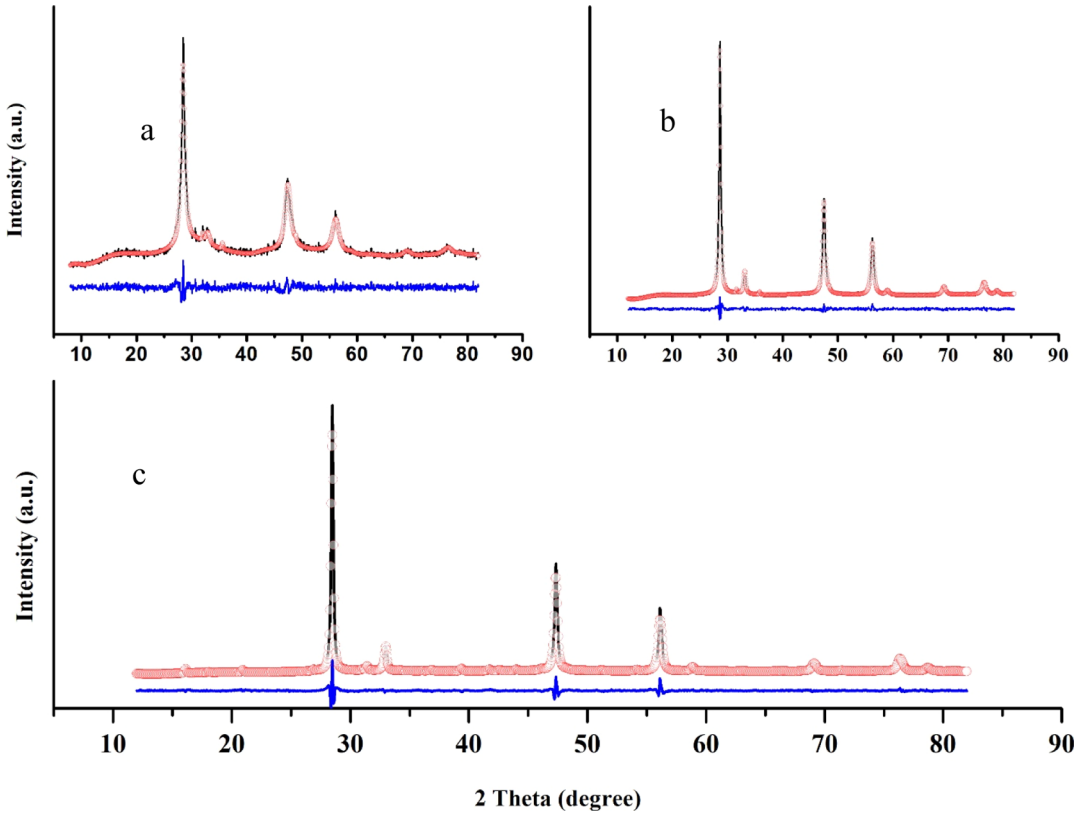

Figure 3. Rietveld refinement performed on 60 min milled powder (a), disordered (b), and ordered (c) sintered CTS samples. Experimental data (circle), model (line) and their difference, or residual (line below).

RESULTS AND DISCUSSION

Structural Analysis. XRD measurements were performed on elemental powder milled for 30 and 60 min, and samples were sintered at 500 and 650 °C (shown in Figure 2). The 30 min milled powder was observed as a blend of partially formed CTS, binary sulfides (SnS and CuS), and metallic elements (Cu and Sn). With a longer milling time of 60 min, the CTS (SG: $F\bar{4}3m$) formation was complete, although one weak Sn peak ($2\theta \sim 32°$) could still be observed. Because of the use of WC vials for the milling, traces of WC (SG: $P\bar{6}m2$) were present in the as-milled powder. Broad peaks with diffuse background for the as-milled powder suggests the presence of small crystalline domains and a possibly amorphous fraction. As expected, the sintering step increases both crystallinity and grain size. The CTS sample sintered at 500 °C shows a disordered cubic structure alike as-milled CTS, identified by three characteristic peaks at $2\theta \sim 28.5$, 47, and 56°, representing planes (111), (220), and (311), respectively. However, the sample sintered at 650 °C shows three additional peaks located at $2\theta \sim 16$, 18, and 21°, respectively, representing planes (110), ($11\bar{1}$), and (021), characteristic of the ordered monoclinic structure (SG: *Cc*).

To confirm the crystallographic structure and to get quantitative information on the crystallite size, the Rietveld refinement[36] was performed using the whole powder pattern modeling[37] approach, as implemented in the recent release of the software TOPAS 7.[38] The underlying assumption is that the crystalline domains are approximated by spheres with a lognormal distribution of diameters. Modeling results are shown in Figure 3 and Table 1.

Table 1. Lattice Parameter and Average Crystallite Size for 60 min Milled Powder, Disordered, and Ordered Sintered CTS Samples (*cf.* Figure 3a,b,c, Respectively)

sample	lattice parameters (±0.01 Å)	angle (deg)	average crystallite size (±10 nm)
60 min milled	$a = b = c = 5.44$	$\alpha = \beta = \gamma = 90$	20
disordered	$a = b = c = 5.44$	$\alpha = \beta = \gamma = 90$	50
ordered	$a = 6.66$, $b = 11.54$, $c = 6.66$	$\alpha = \gamma = 90$, $\beta = 109.39$	200

The formation of tin oxides is a known problem for this family of materials, which deteriorates the TE performance in temperature.[39] These oxide phases are hard to eliminate because of the low partial pressure for tin oxide formation.[40] Comparatively, a higher amount (2−5% weight fraction) of tin oxides was observed in CTS samples prepared using binary sulfides (CuS and SnS). Rather, the present samples prepared from elemental powders (Cu, Sn, and S) processed in a strictly controlled environment do not show the formation of secondary phase oxides in the disordered CTS, which is a substantial improvement from previous studies.[22] Nevertheless, a small amount of SnO_2 (<1% in weights) was observed in the ordered CTS.

Electronic Transport. Figure 4a shows the electrical resistivity and Seebeck coefficient for the CTS polymorphs. Both phases show an overall decreasing trend of resistivity with the temperature, while S has positive values and an increasing trend, typical of nondegenerate p-type semiconductors. Nevertheless, the ordered sample shows a decrease in *S* above ~600 K, likely caused by thermal excitation of bipolarons.[20] The disordered sample presents a lower

https://dx.doi.org/10.1021/acs.jpcc.0c09139
J. Phys. Chem. C 2021, 125, 178−188

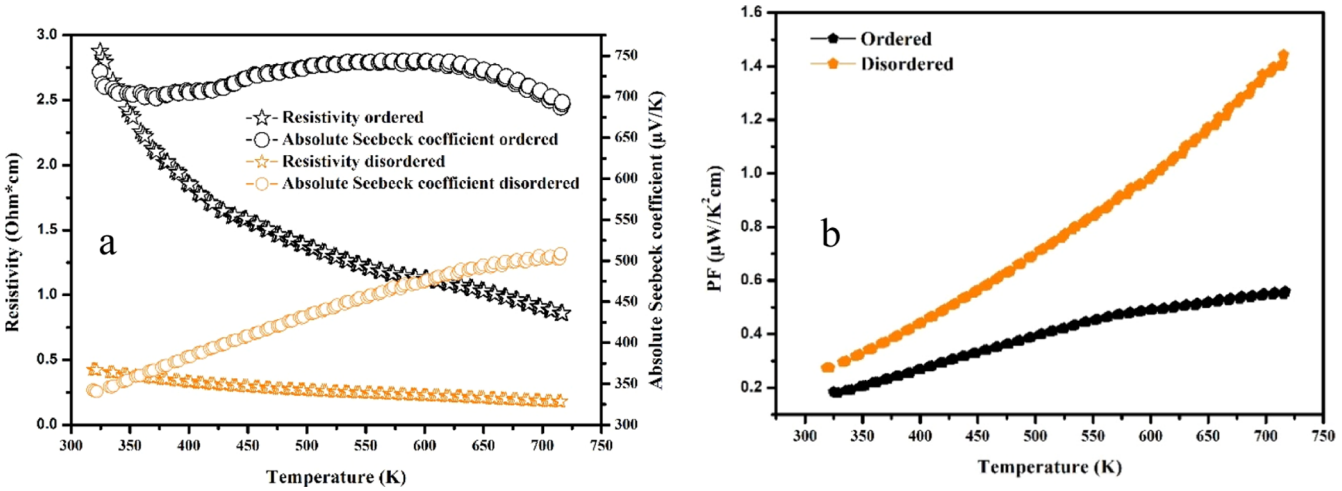

Figure 4. Resistivity (star) and absolute Seebeck coefficient (circle) for ordered (black) and disordered (orange) phases (a); corresponding power factor calculated as PF = S^2/ρ for ordered (black) and disordered (orange) CTS (b).

resistivity ($\rho \sim 0.5-0.2$ Ω cm) than the ordered ($\rho \sim 3.0-1.0$ Ω cm). Optical measurements (Figure 5) show band gaps

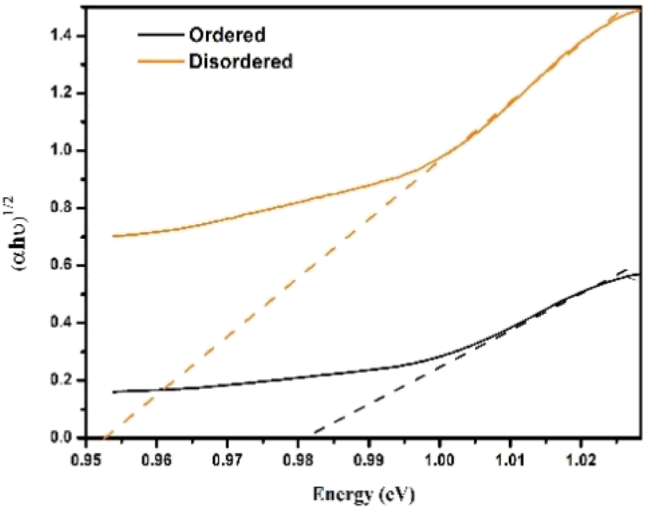

Figure 5. Band gap (E_g) estimated by linear extrapolation in the Tauc plot, using the equation $\alpha h\nu = A(h\nu - E_g)^{1/2}$, where α, h, ν, A, and E_g are absorption coefficient, Planck constant, frequency, transition constant, and band gap, respectively (optical absorption spectra is shown in the Supporting Information file, Figure S1).

~0.99 and ~0.95 eV for the ordered and disordered samples, respectively. A lower band gap promotes a higher carrier concentration, and indeed, the average value of carrier concentration for the disordered sample ($n \sim 1.9 \times 10^{18}$ cm^{-3}) is 10-fold higher than the ordered ($n \sim 2.7 \times 10^{17}$ cm^{-3}). The two polymorphs show similar mobility ($\mu \sim 20$ cm^2/V s) and values compatible with those expected for the stable CTS phase (spanning from 1 to 80 cm^2/V s[41]) (shown in Figure S2, Supporting Information). According to the Mott equation,[2] both n and μ have an inverse relation with the Seebeck coefficient, and this explains the lower S (~320−500 μV/K) for the disordered sample. Overall, above 700 K, the disordered CTS presents a higher PF (~1.5 $\mu W/K^2$ cm) than the ordered polymorph (~0.5 $\mu W/K^2$ cm); see Figure 4b.

In order to further understand the differences between the results obtained for ordered and disordered samples, the electronic properties were investigated by DFT. As already pointed out, the ordered structure was simulated with its exact stoichiometry, using 24-atoms (8-Cu, 4-Sn, and 12-S), whereas for the disordered phase, the constraint of occupancy and the structure[25] led us to simulate two slightly off-stoichiometric structures, Sn-rich (21-Cu, 11-Sn, and 32-S) and Sn-poor (22-Cu, 10-Sn, and 32-S), respectively. Total and atomic projected electronic DOS are shown in Figure 6 for both CTS structures.

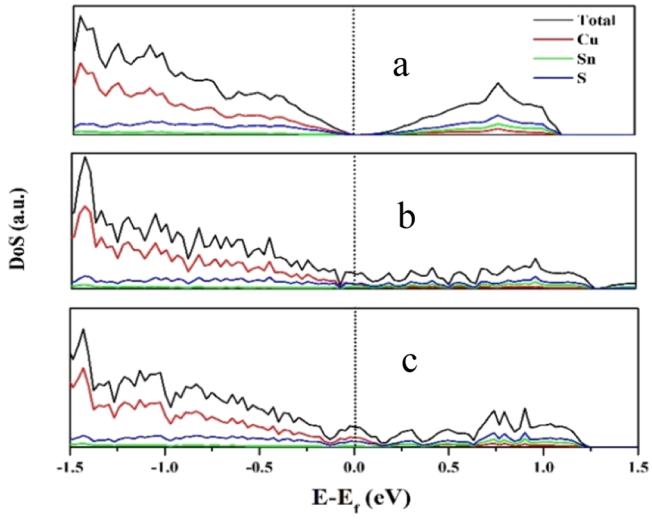

Figure 6. Total DOS and atomic projected DOS for ordered (a), Sn-rich disordered (b), and Sn-poor disordered (c) cells; the Fermi energy is shown by the dotted line.

The total DOS is higher in the valence band (VB) side than in the conduction band (CB), for all the structures, confirming the p-type nature of CTS. In VB, the main contribution to the projected-atomic DOS is given by Cu 3d and S 3p orbitals, whereas the CB is composed of Sn 5s and S 3p orbitals.

Band structures are shown in Figure S3 of the Supporting Information file. This for the ordered CTS is in agreement with the literature,[25,42] also showing a largely underestimated band gap value. This is even more relevant for the cubic phase, where no band gap is observed in the DFT results, as it has also been found for analogous simulations of the disordered copper−tin−selenide system.[28] The random distribution of Cu

https://dx.doi.org/10.1021/acs.jpcc.0c09139
J. Phys. Chem. C 2021, 125, 178−188

and Sn atoms in the disordered structures causes band tailing, which points out the presence of available states in the DOS curve near the Fermi energy.[43] It is likely that the structures in the gap region and the tailing of the DOS at the Fermi energy play a role in enhancing the carrier concentration, as we observed experimentally. Even if the PBE exchange−correlation tends to underestimate the band gap,[44] the band tailing reduces the band gap, in agreement with the optical absorption results of Figure 5.

Thermal Transport. Thermal conductivity was calculated as $k = DdC_p$, where D, d, and C_p are thermal diffusivity, density, and specific heat capacity, respectively. Thermal diffusivity and density were measured using a xenon flash instrument and Archimedes' method, respectively, while the value of C_p was taken from our previous work.[22]

As shown in Figure 7, the thermal conductivity of the ordered CTS ranges from 1.0 to 0.45 W/m K, whereas it is

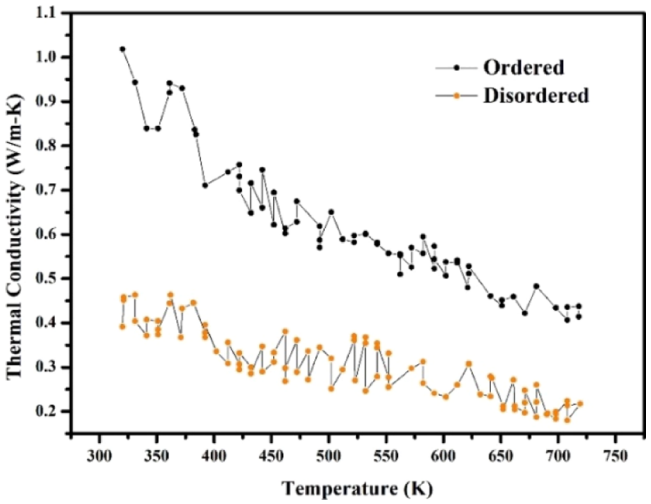

Figure 7. Thermal conductivity for CTS polymorphs in the temperature range of 323−723 K.

ultralow for the disordered CTS, with values 0.45−0.20 W/m K, in the temperature range 323−723 K. The trend of k decreases with temperature, indicative of increased phonon−phonon interactions. The present values of k are lower than in CTS prepared by high-temperature solid-state reactions.[17] Reasons are likely related to the bottom-up production method, which limits the grain growth, as well as to a lower density. However, the effect of the lower density on thermal conductivity can be ignored for the comparison between samples of the two polymorphs because they have similar densities (~3.7 g/cm^3), lower than theoretical (~4.85 g/cm^3). Furthermore, near room temperature (T = 323 K), the lattice component of thermal conductivity was estimated using the single parabolic band (SPB) approximation (calculations used are shown in the Supporting Information file). As it happens in highly resistive semiconductors, the thermal conductivity is dominated by the lattice part. For ordered and disordered samples, the k_l is ~0.44 and ~0.99 W/m K, respectively; such values are close to the experimentally measured values for total thermal conductivity, confirming the main role of phonon contribution to thermal transport. However, the difference between the values achieved by the two samples suggests a relevant discrepancy in the pDOS for the two structures.

The phonon dispersion curves were investigated using first-principle calculations to shed light on the lower k_l of the disordered polymorph. The primitive cell of the ordered CTS has 12 atoms, whereas the disordered cells were simulated with 64 atoms. Therefore, the phonon dispersion curves show 3N (N = number of atoms), 36 and 192, branches of vibrational modes, respectively (see Figure 8a−c). Three low-frequency modes are acoustical, rest (3N-3) of the branches correspond to the optical modes. The low-frequency modes in all three cells are dominated by heavy Cu and Sn, while S, a much lighter atom, dominates the high-frequency modes. The difference in atomic-projected pDOS can be observed in a frequency of <1 THz, in ordered and Sn-poor cells; these modes are dominated by Cu vibrations, whereas Sn vibrations dominate in the Sn-rich cell.[45] The acoustic modes in the disordered Sn-rich cell are softer as compared to the ordered. Additionally, simulations show a weak bonding and a strong anharmonicity along the $\Gamma-X$ and $\Gamma-Z$ directions,[46] whereas these effects are less evident for the Sn-poor cell. The vibrational modes for the disordered cells are shifted to lower frequencies (see Figure 8d), and the gap between low- and high-lying optical modes is narrower with higher population of low-lying optical modes. Moreover, optical modes cut the acoustical modes at a lower (~1.1 THz) frequency in the disordered cells than in the ordered (~1.9 THz), suppressing the lattice thermal conductivity by scattering the heat-carrying acoustic modes.[45]

The optical phonon branches in the disordered cells are flatter than the ordered cell, suggesting a lower group velocity of optical phonons. The mode level phonon group velocity ($V_g = d\omega/dk$) is shown in Figure S4 of the Supporting Information file. The acoustic modes of all three cells show a similar V_g ~ 50 THz Å. However, the experimentally obtained k for the disordered CTS has an approximately twofold lower value than that of the ordered, which cannot be explained in terms of a lower V_g only. This suggests the possibility of heat being trapped in low-velocity optical modes, as discussed with the phonon dispersion curves.[47]

Moreover, a strong anharmonic effect in bonding contributes to a low lattice thermal conductivity. The mode Grüneisen parameter (γ_i), shown for all cells in Figure 9 is a measure of lattice anharmonicity, as it reflects the extent of deviations of phonon vibrations from the harmonic oscillations.

For all cells, the fluctuation in the values of the mode Grüneisen parameter decreases for increasing frequency (shown in the insets of Figure 9), indicating a weak interaction between different vibrations at higher frequencies.[48] The Sn-rich cell shows a much higher mode Grüneisen parameter, whereas comparatively lower values were observed for the ordered and Sn-poor cells, suggesting the anharmonicity in the disordered structures is highly dependent on the concentration of Sn-atoms.

The atomic bonds were investigated by the ELF plots (Figure 10). Cu−S and Sn−S bonds show an ionic and covalent nature, respectively.[49] All Sn-atoms have similar electron localization (Figure 10a) in the ordered cell because of the regular arrangement of S−Cu_2Sn_2 and S−$CuSn_3$ motifs. However, a variation in electron localization is observed in the disordered cells (Figure 10b,c), indicating the inhomogeneous nature of Sn−S bonds[50] (see Figure S5 of the Supporting Information file for the contribution of every Cu and Sn atom to the atomic pDOS). In low frequencies (1−3 THz), an identical contribution of Sn can be observed for the ordered

https://dx.doi.org/10.1021/acs.jpcc.0c09139
J. Phys. Chem. C 2021, 125, 178−188

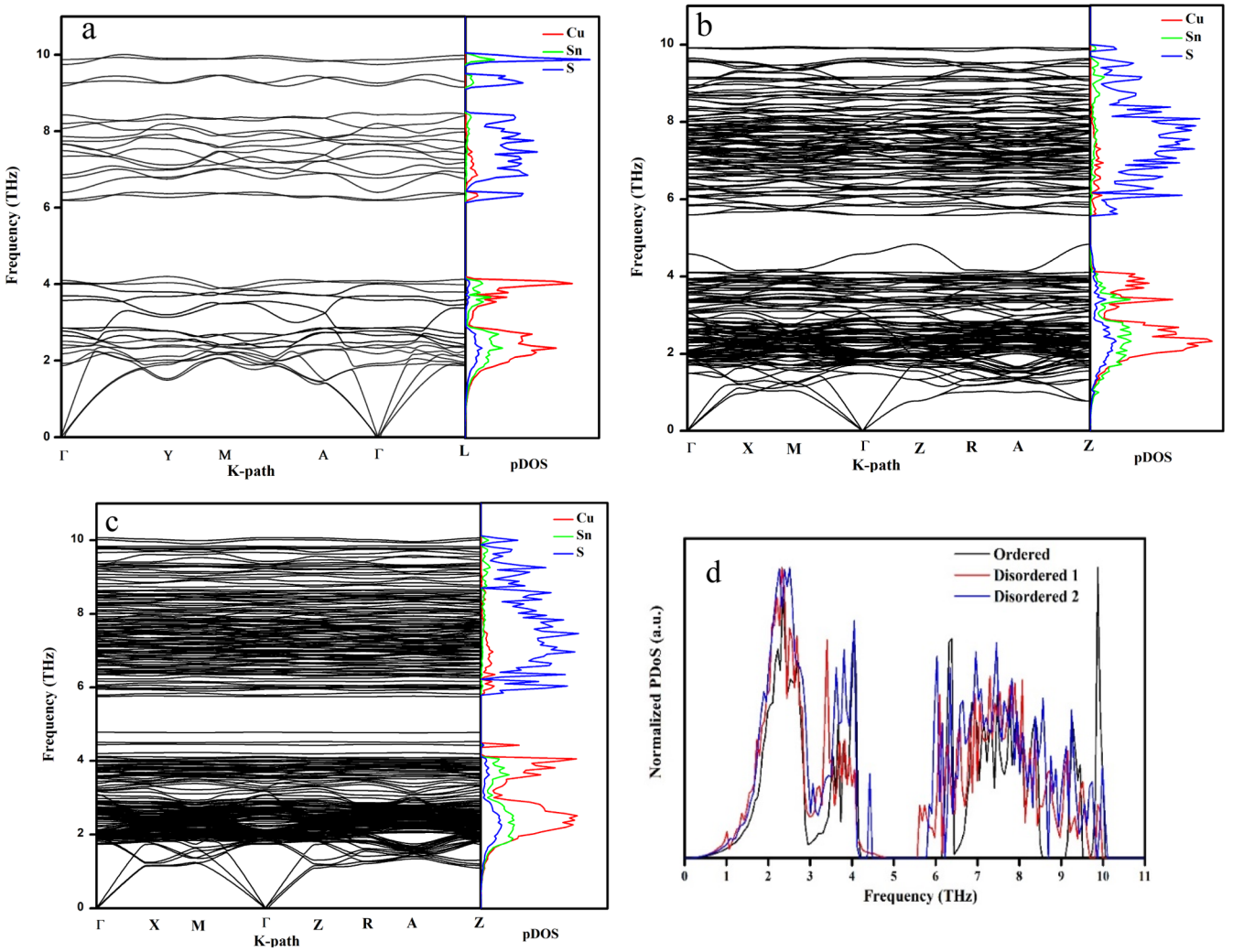

Figure 8. Phonon dispersion curves (ω *vs* k) and atomic-projected pDOS for ordered (a), disordered Sn-rich (b), disordered Sn-poor (c) cells, and a comparison among normalized total pDOS (d).

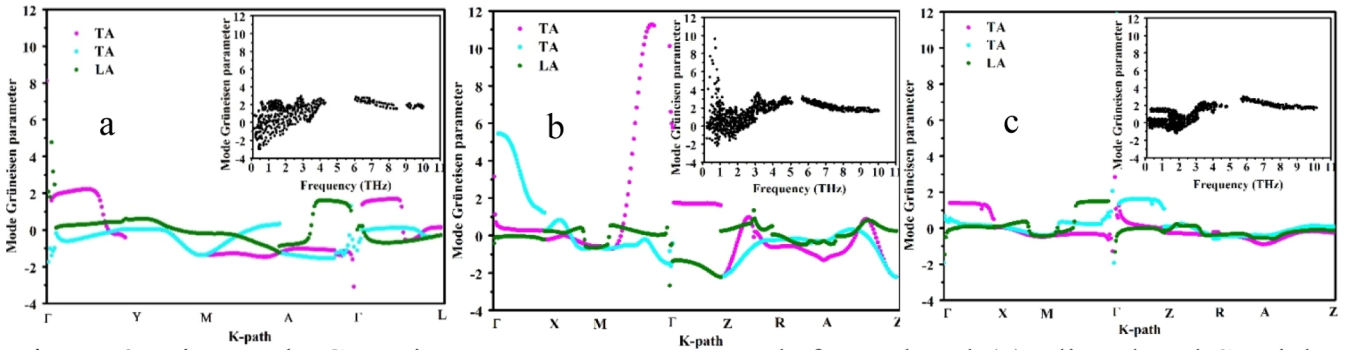

Figure 9. Mode Grüneisen parameter *vs* *K*-path for ordered (a), disordered Sn-rich, (b), and disordered Sn-poor (c) cells; the corresponding Grüneisen parameter *vs* frequency (ω) is shown in the insets.

cell, whereas it is dispersed for disordered cells. These observations suggest a distinct nature of Sn atoms in the disordered cells, that might scatter phonons more efficiently than in the structure of the stable ordered CTS.

To validate the above conclusions on the Sn pDOS obtained by DFPT, NIS experiments (Figure 11) were performed at 43 K on both samples; an additional measurement was performed on the disordered sample at 295 K. The Debye energy was calculated by fitting the reduced pDOS (pDOS/E^2) in the range 0.5−1.2 THz, using the parabolic function, pDOS(E)/E^2 = 3/E_D^3 + bE^2, where E, E_D, and b are energy, Debye energy, and a fitting parameter, respectively.[51] The Debye energy together with other parameters obtained from Sn pDOS are presented in Table 2.

The experimentally observed trend of Sn pDOS at 43 K agrees with the theoretical results for both samples. The disordered sample shows a broad phonon band (5−9 THz), consistently with the atomic-projected pDOS and individual

https://dx.doi.org/10.1021/acs.jpcc.0c09139
J. Phys. Chem. C 2021, 125, 178−188

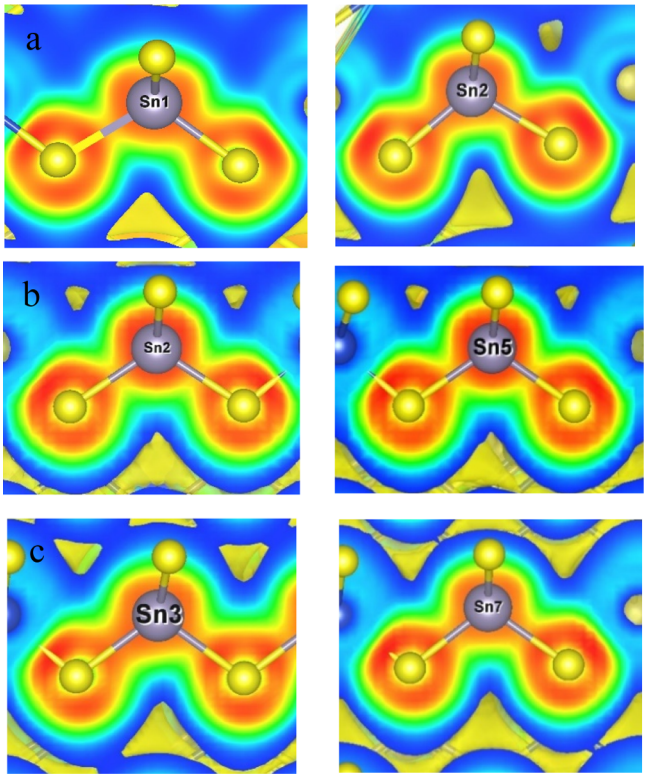

Figure 10. Magnified view of ELF plots for Sn atoms in ordered (a), disordered Sn-rich (b), and disordered Sn-poor (c) cells.

atomic pDOS of Figure 8. The value of the Debye energies and mean sound velocities (see Table 2) are similar for both polymorphs, suggesting similar group velocities, as observed from mode level group velocity calculations.

The NIS measurement performed at 295 K on a disordered CTS sample reveals significant phonon mode softening for the acoustical part of the pDOS and a higher Debye level compared with the low T measurement. The relative energy shifts $\Delta E/E$ of the specific peaks can be obtained from the pDOS measured at 43 and 295 K using the procedure described in refs 52 and 53. XRD measurements were performed from 300 to 100 K with a step of 20 K (shown in the Supporting Information file), and the relative volume change $\Delta V/V = 0.0065$ between 43 and 295 K was estimated by fitting a parabolic function (see Figure 12b). Thus, using both relative volume and energy change Grüneisen parameters for specific phonon peaks were obtained and are shown in Figure 12a, which agrees with the results obtained *via ab initio* calculations presented in Figure 9. In particular, the high Grüneisen parameter was observed for the 0 energy and 4 THz peak. The 0-energy value of the Grüneisen parameter was obtained by comparison of the Debye energy.

Hence, from the analyses performed on the samples and the good agreement achieved with the theoretical calculations, the ultralow thermal conductivity in the disordered sample is shown to be because of the random arrangement of Sn and Cu atoms, which not only blocks the normal phonon scattering but also shows strong anharmonicity for the inhomogeneous nature of the Sn−S bonds. The low-lying optical modes support acoustical-optical phonon scattering, and the higher value of the Grüneisen parameter obtained from DFPT and NIS results confirm the higher anharmonicity in the disordered structure. However, a lower mode Grüneisen parameter was observed in the Sn-poor cell, suggesting that anharmonicity in the disordered system is largely dependent on the Sn-atoms. Moreover, a small crystallite size (<100 nm) and the coexistence of secondary phases (WC, SnO, and SnO_2) should also serve to additional phonon scattering.

The results achieved up to here are well summarized combining the electric and thermal transport properties in the dimensionless figure of merit, zT (Figure 13). For the ordered sample, $zT \sim 0.05$ is in agreement with the values commonly reported in literature,[19] whereas $zT \sim 0.5$ was observed for the disordered CTS polymorphs above 700 K, which is fairly high for an undoped material.[4] In particular, as demonstrated by our results, the enhanced zT for the disordered CTS is an attribute of its high PF and ultralow thermal conductivity.

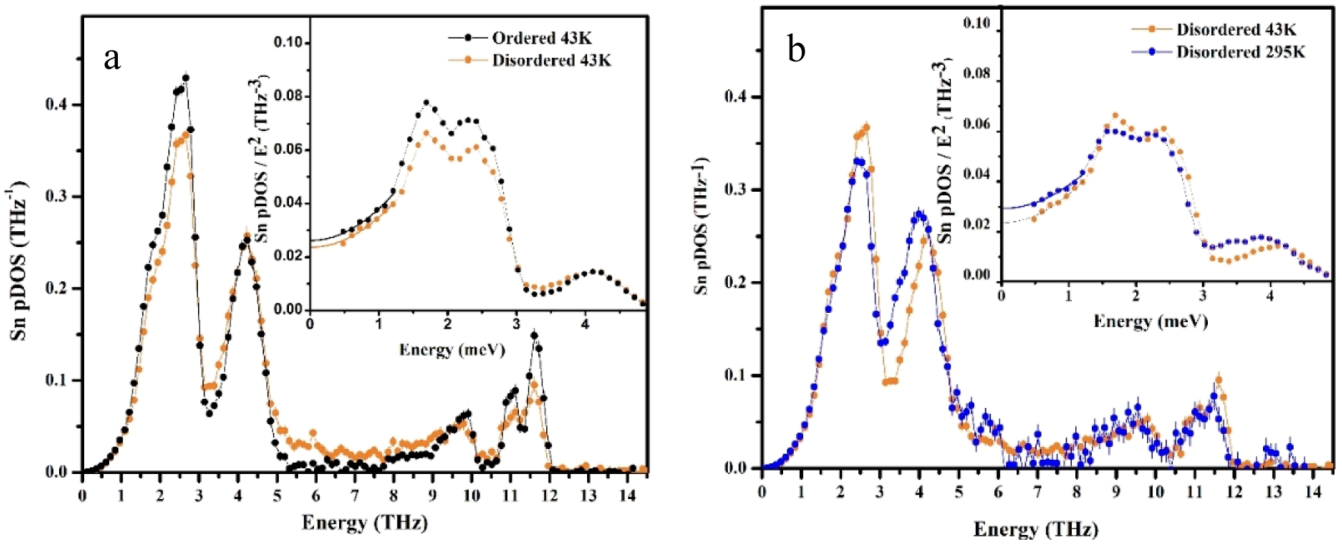

Figure 11. Sn pDOS-ordered and disordered CTS samples at 43 K (a) and disordered CTS samples at 43 and 295 K (b). Reduced Sn pDOS plots are shown in the inset for both figures.

https://dx.doi.org/10.1021/acs.jpcc.0c09139
J. Phys. Chem. C 2021, 125, 178−188

Table 2. Parameters Obtained from the Sn VDOS of the Samples Measured at 43 and 295 K: The Lamb−Mössbauer Factor (f_{LM}), the Sn Atomic Displacement Parameter (U_{eq}), the Mean Force Constant (F), the Debye Energy (E_D), and the Mean Sound Velocity V

	f_{LM}	U_{eq} (A^2)	F (N/m)	E_D (THz)	V (km/s)
ordered at 43 K	0.754(1)	0.00180(2)	224(2)	5.13(5)	2.69
disordered at 43 K	0.769(1)	0.00193(2)	221(1)	5.02(5)	2.81
disordered at 295 K	0.291(4)	0.00844(5)	196(5)	4.67(5)	2.62

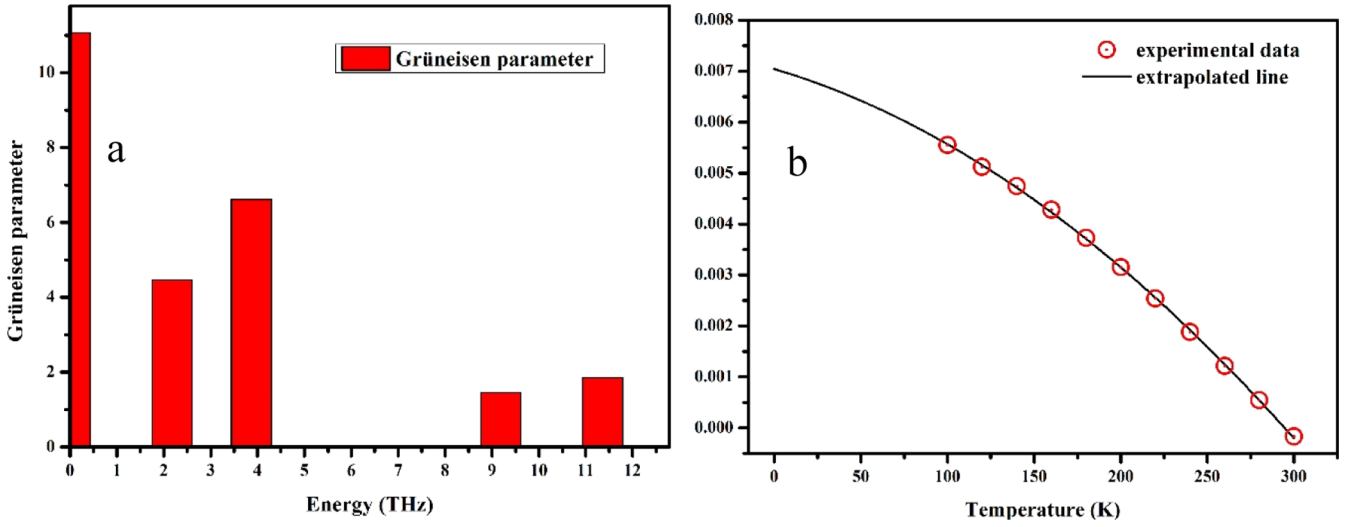

Figure 12. Grüneisen parameters of the specific phonon peaks of the disordered compound obtained from the NIS measurements at 43 and 295 K (a) and relative volume change $\Delta V/V_{295K}$ from the XRD data collected in temperature range 300−100 K (b).

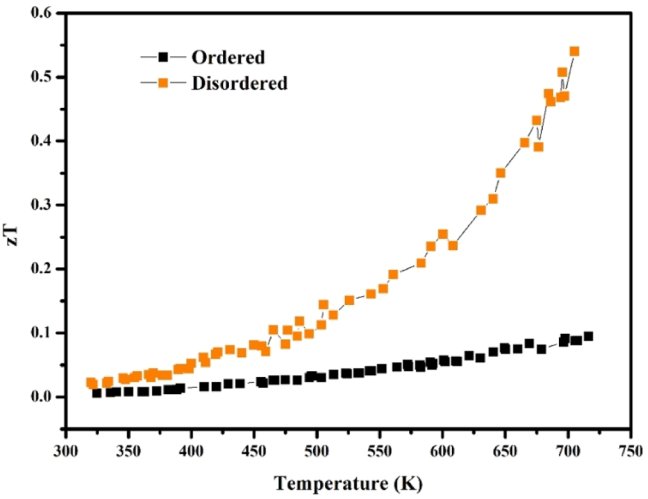

Figure 13. Calculated zT for ordered and disordered CTS samples.

CONCLUSIONS

In this work, a study of the dependence of TE properties of CTS by structural characteristics has been presented. In particular, the effect of structural disorder on electronic and thermal transport properties have been investigated, taking advantage of different experimental techniques. The disordered CTS polymorph shows a better TE performance than the ordered and stable CTS phase, mainly because of an enhanced carrier concentration and ultralow thermal conductivity observed in the former phase. In the present study, we have experimentally determined Seebeck coefficient, resistivity, and thermal conductivity and correlated them with the band gap, mobility, and carrier concentration obtained also from experimental measurements.

First-principle simulations disclose the presence of low-lying optical modes in the disordered cubic structure, with significant variation in the Sn bonding, leading to a strong anharmonicity. A variation in values of the mode Grüneisen parameter for Sn-rich and Sn-poor disordered cells confirms that the anharmonicity is dependent on the Sn-atoms. The overall picture emerging from DFT and DFPT simulations finds confirmation in NIS experiments, as the Sn-pDOS is in agreement with the *ab initio* results. NIS experiments performed at low (43 K) and near-room temperature (295 K) show evidence of a strong anharmonicity, presence of softer modes, and a higher Debye level in the disordered polymorph. The results presented in this work cover most of the material characteristics providing a detailed understanding of the mechanisms promoting a relevant improvement in TE properties of CTS-based materials. In particular, the structural disorder results to have a major impact on the enhancement of material performance. Therefore, these results suggest the strategy for the design of novel solutions for the development of materials based on CTS with improved TE properties.

ASSOCIATED CONTENT

Supporting Information

The Supporting Information is available free of charge at https://pubs.acs.org/doi/10.1021/acs.jpcc.0c09139.

Optical absorption spectra; carrier concentration (n) and mobility (μ) plots; band structures; mode level group velocity; each Sn and Cu atom contribution in individual pDOS; lattice thermal conductivity(k_l) calculations using SPB approximation; and high-

https://dx.doi.org/10.1021/acs.jpcc.0c09139
J. Phys. Chem. C 2021, 125, 178−188

resolution XRD studies in temperature range 295−100 K (PDF)

AUTHOR INFORMATION

Corresponding Author

Paolo Scardi − *Department of Civil, Environmental & Mechanical Engineering, University of Trento, 38123 Trento, Italy;* orcid.org/0000-0003-1097-3917; Email: Paolo.Scardi@unitn.it

Authors

Ketan Lohani − *Department of Civil, Environmental & Mechanical Engineering, University of Trento, 38123 Trento, Italy;* orcid.org/0000-0003-2103-4130

Himanshu Nautiyal − *Department of Civil, Environmental & Mechanical Engineering, University of Trento, 38123 Trento, Italy*

Narges Ataollahi − *Department of Civil, Environmental & Mechanical Engineering, University of Trento, 38123 Trento, Italy*

Carlo Fanciulli − *National Research Council of Italy-Institute of Condensed Matter Chemistry and Technologies for Energy (CNR-ICMATE), 23900 Lecco, Italy*

Ilya Sergueev − *Deutsches Elektronen-Synchrotron DESY, D-22607 Hamburg, Germany*

Martin Etter − *Deutsches Elektronen-Synchrotron DESY, D-22607 Hamburg, Germany*

Complete contact information is available at: https://pubs.acs.org/10.1021/acs.jpcc.0c09139

Notes

The authors declare no competing financial interest.

ACKNOWLEDGMENTS

The authors are thankful to Eleonora Isotta, Binayak Mukherjee, Dr. Raju Edla, and Dr. Mirco D'Incau for useful help and suggestions. We are grateful to the Jülich Supercomputing Centre (JSC), Germany for computational resources. This research was funded by the Autonomous Province of Trento for the support provided within the framework of the programmatic Energy Action 2015−2017.

REFERENCES

(1) Snyder, G. J.; Toberer, E. S. Complex Thermoelectric Materials. *Nat. Mater.* **2008**, *7*, 105−114.

(2) Mao, J.; Liu, Z.; Zhou, J.; Zhu, H.; Zhang, Q.; Chen, G.; Ren, Z. Advances in Thermoelectrics. *Adv. Phys.* **2018**, *67*, 69−147.

(3) Sootsman, J. R.; Chung, D. Y.; Kanatzidis, M. G. New and Old Concepts in Thermoelectric Materials. *Angew. Chem., Int. Ed.* **2009**, *48*, 8616−8639.

(4) Han, C.; Sun, Q.; Li, Z.; Dou, S. X. Thermoelectric Enhancement of Different Kinds of Metal Chalcogenides. *Adv. Energy Mater.* **2016**, *6*, 1600498.

(5) Mao, J.; Liu, Z.; Ren, Z. Size Effect in Thermoelectric Materials. *npj Quantum Mater.* **2016**, *1*, 16028.

(6) Mehta, R. J.; Zhang, Y.; Karthik, C.; Singh, B.; Siegel, R. W.; Borca-Tasciuc, T.; Ramanath, G. A New Class of Doped Nanobulk High-Figure-of-Merit Thermoelectrics by Scalable Bottom-up Assembly. *Nat. Mater.* **2012**, *11*, 233−240.

(7) Ibáñez, M.; Luo, Z.; Genç, A.; Piveteau, L.; Ortega, S.; Cadavid, D.; Dobrozhan, O.; Liu, Y.; Nachtegaal, M.; Zebarjadi, M.; et al. A. High-Performance Thermoelectric Nanocomposites from Nanocrystal Building Blocks. *Nat. Commun.* **2016**, *7*, 10766.

(8) Kovalenker, V. A. CU2SNS3, a New Sulfide of Tin and Copper. *Int. Geol. Rev.* **1983**, *25*, 117−120.

(9) Fernandes, P. A.; Salomé, P. M. P.; Cunha, A. F. D. A Study of Ternary Cu2SnS3 and Cu3SnS 4 Thin Films Prepared by Sulfurizing Stacked Metal Precursors. *J. Phys. D: Appl. Phys.* **2010**, *43*, 215403.

(10) Fernandes, P. A.; Salomé, P. M. P.; Da Cunha, A. F. CuxSnSx +1 (x = 2, 3) Thin Films Grown by Sulfurization of Metallic Precursors Deposited by Dc Magnetron Sputtering. *Phys. Status Solidi C* **2010**, *7*, 901−904.

(11) Pallavolu, M. R.; Minnam Reddy, V. R.; Pejjai, B.; Jeong, D.-s.; Park, C. Effect of Sulfurization Temperature on the Phase Purity of Cu 2 SnS 3 Thin Films Deposited via High Vacuum Sulfurization. *Appl. Surf. Sci.* **2018**, *462*, 641−648.

(12) Chen, Q.; Maeda, T.; Wada, T. Optical Properties and Electronic Structures of Cu2SnS3, Cu2GeS3, and Their Solid Solution Cu2(Ge,Sn)S3. *Jpn. J. Appl. Phys.* **2018**, *57*, 08RC20.

(13) Raadik, T.; Grossberg, M.; Krustok, J.; Kauk-Kuusik, M.; Crovetto, A.; Bolt Ettlinger, R.; Hansen, O.; Schou, J. Temperature Dependent Photoreflectance Study of Cu2SnS3 Thin Films Produced by Pulsed Laser Deposition. *Appl. Phys. Lett.* **2017**, *110*, 261105.

(14) Xi, L.; Zhang, Y. B.; Shi, X. Y.; Yang, J.; Shi, X.; Chen, L. D.; Zhang, W.; Yang, J.; Singh, D. J. Chemical Bonding, Conductive Network, and Thermoelectric Performance of the Ternary Semiconductors Cu 2 SnX 3 (X= Se, S) from First Principles. *Phys. Rev. B: Condens. Matter Mater. Phys.* **2012**, *86*, 155201.

(15) Tan, Q.; Sun, W.; Li, Z.; Li, J.-F. Enhanced Thermoelectric Properties of Earth-Abundant Cu2SnS3 via In Doping Effect. *J. Alloys Compd.* **2016**, *672*, 558−563.

(16) Shen, Y.; Li, C.; Huang, R.; Tian, R.; Ye, Y.; Pan, L.; Koumoto, K.; Zhang, R.; Wan, C.; Wang, Y. Eco-Friendly p-Type Cu2SnS3 Thermoelectric Material: Crystal Structure and Transport Properties. *Sci. Rep.* **2016**, *6*, 32501.

(17) Zhang, Z.; Zhao, H.; Wang, Y.; Hu, X.; Lyu, Y.; Cheng, C.; Pan, L.; Lu, C. Role of Crystal Transformation on the Enhanced Thermoelectric Performance in Mn-Doped Cu2SnS3. *J. Alloys Compd.* **2019**, *780*, 618−625.

(18) Xu, X.; Zhao, H.; Hu, X.; Pan, L.; Chen, C.; Li, D.; Wang, Y. Synergistic Role of Ni-Doping in Electrical and Phonon Transport Properties of Cu2Sn1-XNixS3. *J. Alloys Compd.* **2017**, *728*, 701−708.

(19) Zhao, L.; Chen, C.; Pan, L.; Hu, X.; Lu, C.; Wang, Y. Magnetic Iron Doping in Cu2SnS3 Ceramics for Enhanced Thermoelectric Transport Properties. *J. Appl. Phys.* **2019**, *125*, 095107.

(20) Zhao, H.; Xu, X.; Li, C.; Tian, R.; Zhang, R.; Huang, R.; Lyu, Y.; Li, D.; Hu, X.; Pan, L.; et al. Cobalt-Doping in Cu2SnS3: Enhanced Thermoelectric Performance by Synergy of Phase Transition and Band Structure Modification. *J. Mater. Chem. A* **2017**, *5*, 23267−23275.

(21) Oliva, F.; Arqués, L.; Acebo, L.; Guc, M.; Sánchez, Y.; Alcobé, X.; Pérez-Rodríguez, A.; Saucedo, E.; Izquierdo-Roca, V. Characterization of Cu2SnS3 Polymorphism and Its Impact on Optoelectronic Properties. *J. Mater. Chem. A* **2017**, *5*, 23863−23871.

(22) Lohani, K.; Isotta, E.; Ataollahi, N.; Fanciulli, C.; Chiappini, A.; Scardi, P. Ultra-Low Thermal Conductivity and Improved Thermoelectric Performance in Disordered Nanostructured Copper Tin Sulphide (Cu2SnS3, CTS). *J. Alloys Compd.* **2020**, *830*, 154604.

(23) Baranowski, L. L.; McLaughlin, K.; Zawadzki, P.; Lany, S.; Norman, A.; Hempel, H.; Eichberger, R.; Unold, T.; Toberer, E. S.; Zakutayev, A. Effects of Disorder on Carrier Transport in Cu2SnS3. *Phys. Rev. Appl.* **2015**, *4*, 044017.

(24) Zawadzki, P.; Zakutayev, A.; Lany, S. Entropy-Driven Clustering in Tetrahedrally Bonded Multinary Materials. *Phys. Rev. Appl.* **2015**, *3*, 034007.

(25) Zhai, Y.-T.; Chen, S.; Yang, J. H.; Xiang, H. J.; Gong, X. G.; Walsh, A.; Kang, J.; Wei, S. H. Structural Diversity and Electronic Properties of Cu2SnX 3 (X=S, Se): A First-Principles Investigation. *Phys. Rev. B: Condens. Matter Mater. Phys.* **2011**, *84*, 075213.

(26) Crovetto, A.; Chen, R.; Ettlinger, R. B.; Cazzaniga, A. C.; Schou, J.; Persson, C.; Hansen, O. Dielectric Function and Double Absorption Onset of Monoclinic Cu2SnS3: Origin of Experimental

Features Explained by First-Principles Calculations. *Sol. Energy Mater. Sol. Cells* **2016**, *154*, 121−129.
(27) Chen, Q.; Maeda, T.; Wada, T. Optical Properties and Electronic Structures of Cu 2 SnS 3 , Cu 2 GeS 3 , and Their Solid Solution. *Jpn. J. Appl. Phys.* **2018**, *57*, 08rc20.
(28) Siyar, M.; Cho, J.-Y.; Youn, Y.; Han, S.; Kim, M.; Bae, S.-H.; Park, C. Effect of Annealing Temperature on the Phase Transition, Band Gap and Thermoelectric Properties of Cu2SnSe3. *J. Mater. Chem. C* **2018**, *6*, 1780−1788.
(29) Kresse, G.; Furthmüller, J. Efficient Iterative Schemes for Ab Initio Total-Energy Calculations Using a Plane-Wave Basis Set. *Phys. Rev. B: Condens. Matter Mater. Phys.* **1996**, *54*, 11169−11186.
(30) Kresse, G.; Furthmüller, J. Efficiency of Ab-Initio Total Energy Calculations for Metals and Semiconductors Using a Plane-Wave Basis Set. *Comput. Mater. Sci.* **1996**, *6*, 15−50.
(31) Perdew, J. P.; Burke, K.; Ernzerhof, M. Generalized Gradient Approximation Made Simple. *Phys. Rev. Lett.* **1996**, *77*, 3865−3868.
(32) Pack, J. D.; Monkhorst, H. J. "special Points for Brillouin-Zone Integrations"-a Reply. *Phys. Rev. B: Solid State* **1977**, *16*, 1748−1749.
(33) Hinuma, Y.; Pizzi, G.; Kumagai, Y.; Oba, F.; Tanaka, I. Band Structure Diagram Paths Based on Crystallography. *Comput. Mater. Sci.* **2017**, *128*, 140−184.
(34) Togo, A.; Tanaka, I. First Principles Phonon Calculations in Materials Science. *Scr. Mater.* **2015**, *108*, 1−5.
(35) Perdew, J. P.; Zunger, A. Self-Interaction Correction to Density-Functional Approximations for Many-Electron Systems. *Phys. Rev. B: Condens. Matter Mater. Phys.* **1981**, *23*, 5048−5079.
(36) Mccusker, L. B.; Von Dreele, R. B.; Scardi, P.; Cox, D. E.; Loue, D. Rietveld Refinement Guidelines. *J. Appl. Crystallogr.* **1999**, *32*, 36−50.
(37) Scardi, P.; Azanza Ricardo, C. L.; Perez-Demydenko, C.; Coelho, A. A. Whole Powder Pattern Modelling Macros for TOPAS. *J. Appl. Crystallogr.* **2018**, *51*, 1752−1765.
(38) Coelho, A. A. TOPAS and TOPAS-Academic: An Optimization Program Integrating Computer Algebra and Crystallographic Objects Written in C++. *J. Appl. Crystallogr.* **2018**, *51*, 210−218.
(39) Isotta, E.; Fanciulli, C.; Pugno, N. M.; Scardi, P. Effect of the Order-Disorder Transition on the Seebeck Coefficient of Nanostructured Thermoelectric Cu2ZnSnS4. *Nanomaterials* **2019**, *9*, 762.
(40) Isotta, E.; Mukherjee, B.; Fanciulli, C.; Pugno, N. M.; Scardi, P. Order-Disorder Transition in Kesterite Cu2ZnSnS4: Thermopower Enhancement via Electronic Band Structure Modification. *J. Phys. Chem. C* **2020**, *124*, 7091.
(41) Tiwari, D.; Koehler, T.; Klenk, R.; Fermin, D. J. Solution Processed Single-Phase Cu 2 SnS 3 Films: Structure and Photovoltaic Performance. *Sustainable Energy Fuels* **2017**, *1*, 899−906.
(42) Shigemi, A.; Maeda, T.; Wada, T. First-Principles Calculation of Cu2SnS3 and Related Compounds. *Phys. Status Solidi B* **2015**, *252*, 1230−1234.
(43) Baranowski, L. L. Effects of Disorder on Carrier Transport in Cu2SnS3. *Phys. Rev. Appl.* **2015**, *4*, 044017.
(44) Gajaria, T. K.; Dabhi, S. D.; Jha, P. K. Ab Initio Energetics and Thermoelectric Profiles of Gallium Pnictide Polytypes. *Sci. Rep.* **2019**, *9*, 5884.
(45) Lin, S.; Li, W.; Li, S.; Zhang, X.; Chen, Z.; Xu, Y.; Chen, Y.; Pei, Y. High Thermoelectric Performance of Ag9GaSe6 Enabled by Low Cutoff Frequency of Acoustic Phonons. *Joule* **2017**, *1*, 816−830.
(46) Zhao, L.-D.; Lo, S.-H.; Zhang, Y.; Sun, H.; Tan, G.; Uher, C.; Wolverton, C.; Dravid, V. P.; Kanatzidis, M. G. Ultralow Thermal Conductivity and High Thermoelectric Figure of Merit in SnSe Crystals. *Nature* **2014**, *508*, 373−377.
(47) Toberer, E. S.; Baranowski, L. L.; Dames, C. Advances in Thermal Conductivity. *Annu. Rev. Mater. Res.* **2012**, *42*, 179−209.
(48) Zhang, S.; Xu, B.; Lin, Y.; Nan, C.; Liu, W. First-Principles Study of the Layered Thermoelectric Material TiNBr. *RSC Adv.* **2019**, *9*, 12886.
(49) Zhang, R.; Wen, X.; Xu, F.; Zhang, Q.; Sun, L. A Density Functional Theory Study of the Cu 2 ZnSnS 4 Monolayer as a Photo-Electrointegrated Catalyst for Water Splitting and Hydrogen Evolution. *J. Phys. Chem. C* **2020**, *124*, 11922−11929.
(50) Grin, Y. Inhomogeneity and Anisotropy of Chemical Bonding and Thermoelectric Properties of Materials. *J. Solid State Chem.* **2019**, *274*, 329−336.
(51) Bessas, D.; Sergueev, I.; Wille, H. C.; Peron, J.; Ebling, D.; Hermann, R. P. Lattice Dynamics in Bi2Te3 and Sb2Te 3: Te and Sb Density of Phonon States. *Phys. Rev. B: Condens. Matter Mater. Phys.* **2012**, *86*, 224301.
(52) Sergueev, I.; Hermann, R. P.; Bessas, D.; Pelzer, U.; Angst, M.; Schweika, W.; McGuire, M. A.; Sefat, A. S.; Sales, B. C.; Mandrus, D.; et al. Effect of Pressure, Temperature, Fluorine Doping, and Rare Earth Elements on the Phonon Density of States of LFeAsO Studied by Nuclear Inelastic Scattering. *Phys. Rev. B: Condens. Matter Mater. Phys.* **2013**, *87*, 064302.
(53) Sergueev, I.; Glazyrin, K.; Kantor, I.; McGuire, M. A.; Chumakov, A. I.; Klobes, B.; Sales, B. C.; Hermann, R. P. Quenching Rattling Modes in Skutterudites with Pressure. *Phys. Rev. B: Condens. Matter Mater. Phys.* **2015**, *91*, 224304.

https://dx.doi.org/10.1021/acs.jpcc.0c09139
J. Phys. Chem. C 2021, 125, 178−188